Mechanism of Structural Formation by Uniaxial Deformation in Amorphous Poly(ethylene terephthalate) above the Glass Temperature

Daisuke Kawakami, Shaofeng Ran, Christian Burger, Bruce Fu, Igors Sics, Benjamin Chu, and Benjamin S. Hsiao*

Department of Chemistry, State University of New York at Stony Brook, Stony Brook, New York 11794-3400

Received June 10, 2003
Revised Manuscript Received September 24, 2003

1. Introduction. Recently, several research groups have investigated the role of the mesophase in crystallization of oriented poly(ethylene terephthalate) (PET). For example, Windle and co-workers studied the formation of a transient smectic phase in the fiber of random PET and PEN (polyethylene naphthalene-2,6-dicarboxylate) copolymers.[1] Blundell and co-workers investigated the in situ structural development of PET films during fast-drawing using synchrotron X-ray techniques.[2] Asano and co-workers reported the appearance of a mesophase during isothermal annealing of cold drawn PET.[3] Hsiao and co-workers studied the deformation and subsequent crystallization of amorphous PET film during stretching below the glass transition temperature (T_g) also using synchrotron X-rays.[4] All these groups reported that the deformation-induced mesomorphic structure in PET is a precursor for crystallization. These findings are somewhat consistent with the recent hypothesis proposed by Strobl.[5] He proposed that the initial step in crystallization is the creation of a mesomorphic layer that spontaneously thickens to a critical value, where it solidifies through a cooperative structural transition. The transition produces a granular crystalline layer, which transforms in the last step into homogeneous lamellar crystallites. However, we believe that the detailed mechanism in orientation-induced crystallization of PET may be different from the Strobl's model. The current study (deformation above T_g) was carried out as a continuing effort to understand this difference and the exact role of the mesophase in the crystallization of oriented PET.

Deformation studies of amorphous PET above its T_g are relatively rare because of the experimental difficulties at high temperatures.[1,2,6,7] The typical study dealing with this subject was usually carried out in two steps (we termed this step-quenching process): (1) deformation at high temperatures and (2) subsequent quenching to preserve the structure in the deformed sample for characterization. Using this technique, Salem studied the relationship between the structure formation and the property development in PET and proposed a two-stage mechanism: (1) the initial stage involves the development of stress increase and fast crystallization; (2) the second stage involves a dramatic increase of stress (strain-hardening) and moderate crystallinity increase.[6] Gorlier et al. also investigated the deformation process of PET above T_g using a similar technique, but they classified the relationships between the structural formation and the property development in three stages.[7] In the first stage, molecular orientation occurs due to strong molecular interactions. In the second stage, nuclei appear as a result of molecular orientation. (At a given level of strain, the number of nuclei is fixed, which forms a network structure that can induce strain hardening.) In the last stage, crystallization develops through the growth process.

There are clearly some inconsistencies in the understanding of the relationship between structure and mechanical properties in the deformation-induced crystallization of PET above T_g, in addition to the missing role of the mesophase. These form the basis for this study. As we are concerned that during the step-quenching process some additional changes in structure and morphology are inevitable, an in situ study of the structural formation of amorphous PET during uniaxial deformation above T_g (90 °C) was carried out using synchrotron wide-angle X-ray diffraction (WAXD). We have paid special attention to the relationship between the load−strain curve and the formation of the mesomorphic structure. On the basis of our results, a new three-zone mechanism was proposed.

2. Experimental Section. Sample Preparation. The PET sample was an experimental material prepared by Toray Co., Ltd. Minimum amounts of catalyst for polycondensation and of phosphate compound for heat durability were included. No other additives were used. The sample was dried in a vacuum oven at 150 °C for 6 h after first being annealed at 120 °C for 3 h, and then was molded into a dumbbell-shape at 270 °C followed by rapid quenching with ice water. The molded sample dimensions were 25 mm in length, 6 mm in width, and 1 mm in thickness. The final molecular weight (M_w) of the molded sample was about 25 000 g/mol and the polydispersity (M_w/M_n) was about 2.0. The molded sample was completely amorphous without detectable crystallinity by X-ray and DSC.

Synchrotron Measurements. Synchrotron X-ray measurements were performed at the X3A2 Beamline in the National Synchrotron Light Source (NSLS), Brookhaven National Laboratory (BNL). The wavelength was 1.54 Å. A three-pinhole collimator system was used to reduce the beam diameter to 0.6 mm.[8] A modified Instron 4410 was used, which contained a symmetrical stretching unit enabling the focused beam to illuminate the same position of the sample during deformation. Two-dimensional WAXD patterns were accumulated for periods of 20 s (per 6.7% strain) using a MAR CCD X-ray detector (MAR USA). The sample-to-detector distance was 114 mm. The diffraction angle was calibrated by using a polypropylene standard and an Al_2O_3 standard from the National Institute of Standards and Technology (NIST). During the deformation measurements, the sample was mounted carefully in the environmental chamber of the Instron apparatus, which was heated by a dry hot nitrogen flow. The sample was kept in the heated chamber for 3 min for equilibrium after reaching 90 °C, before the engagement of tensile deformation. The deformation process was continued until the sample broke (deformation rate was 20% strain/min). Because the sample had a dumbbell shape, there was a slight deviation between the local

* To whom correspondence should be addressed. Telephone: 631-632-7793; Fax: 631-632-6518; E-mail: bhsiao@notes.cc.sunysb.edu.

10.1021/ma034791b CCC: $25.00
Published on Web 11/15/2003

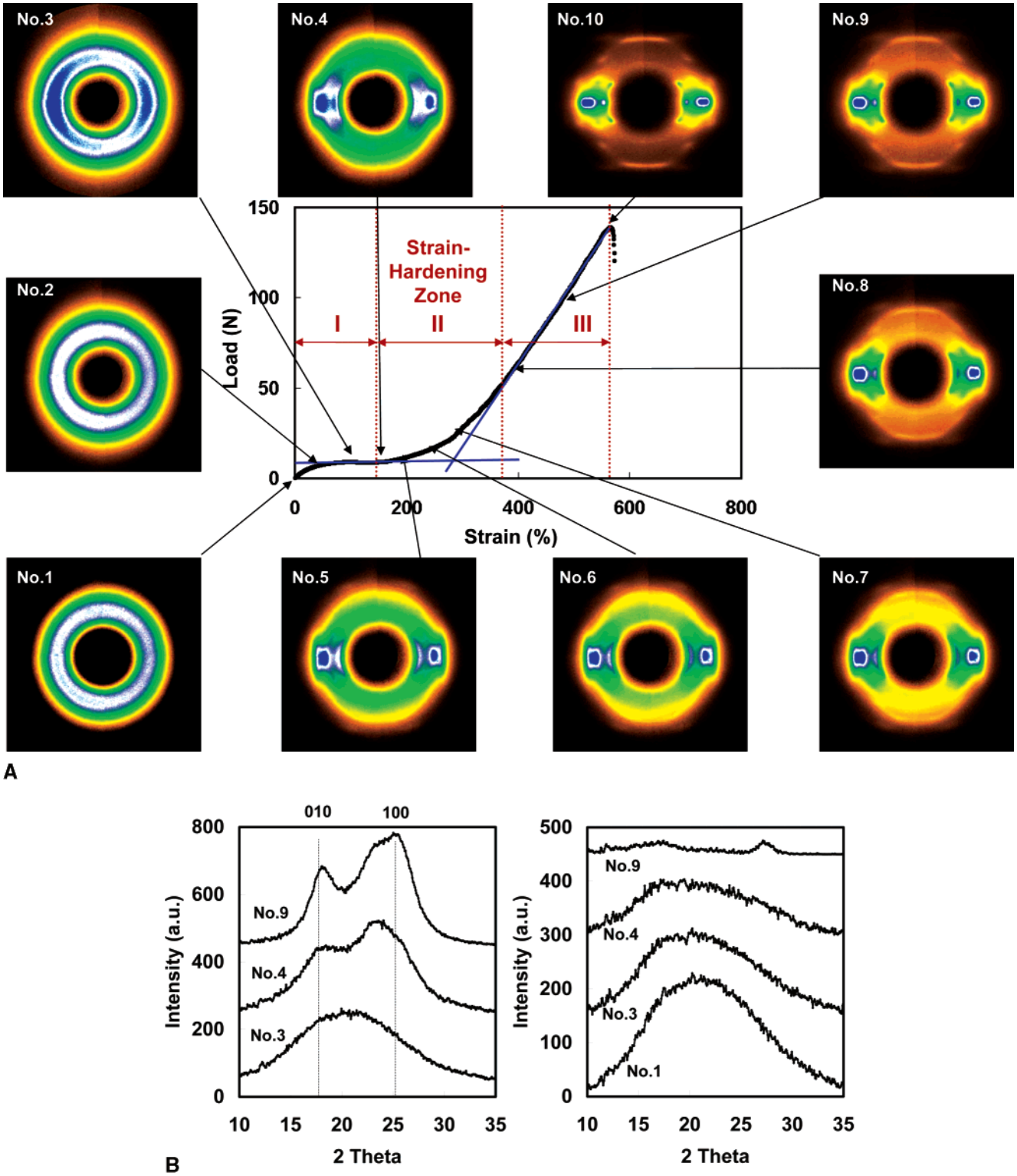

Figure 1. A. Load−strain relationship and selected WAXD patterns collected during stretching. Each image was taken at the average strain indicated by the arrows. B. Equatorial and meridional intensity profiles extracted from selected 2D WAXD patterns. Key: (left) equatorial scans from no. 3, no. 4, and no. 9; (right) meridional scans from no. 1, no. 3, no. 4, and no. 9.

strain and the total strain. This small deviation does not affect the basic understanding of the relationship between structure and mechanical property during the deformation of PET in this study.

3. Results and Discussion. The load−strain curve and selected WAXD patterns through the face-on direction taken during uniaxial deformation of PET at 90 °C are shown in Figure 1A. The arrows indicate the average strain value where each WAXD image was taken. In the conventional view, the determination of the strain-hardening point on the load−strain curve is made by the interception of two extrapolated lines: one fitting the load−strain curve in the low strain region excluding the initial load increase at strain less than 50%, and the other fitting the load−strain curve in the high strain region (Figure 1A). This approach is not consistent with the structure evolution observed by the in situ WAXD patterns. For one thing, there was no abrupt phase

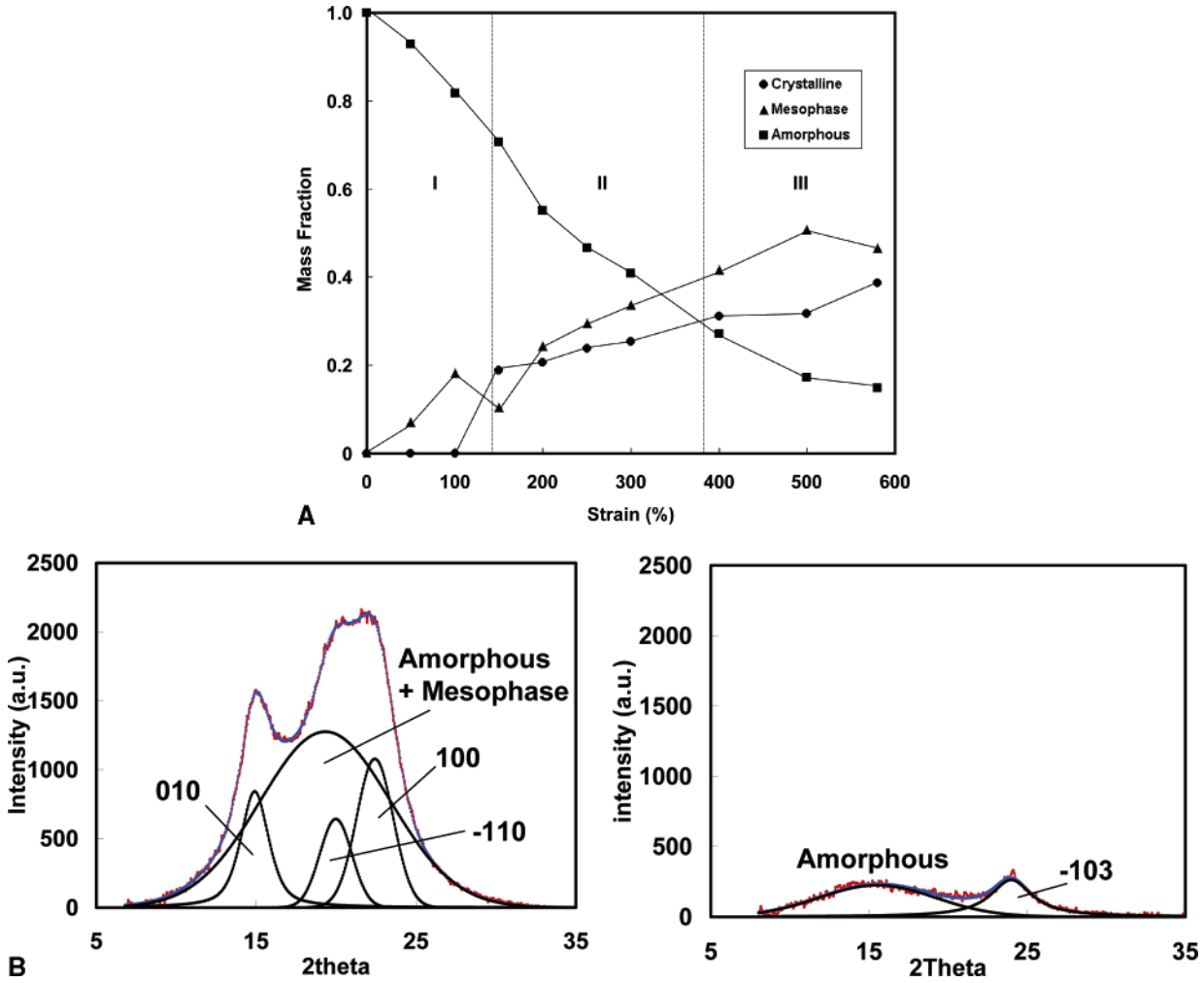

Figure 2. A. Mass fractions of oriented crystalline phase, oriented mesophase and unoriented amorphous phase extracted from the two linear intensity profiles.[11] B. Peak fitting of equatorial (left) and meridional (right) intensity profiles extracted from the 2D WAXD pattern of no. 9.

transition at the strain-hardening point (the crystallization occurred much earlier than the strain-hardening point). A more proper way to correlate the structure and the strain-hardening behavior is by using the definition of a "strain-hardening zone," which starts from the final deviation point of the fitted line in the low strain region and ends with the first deviation point of the fitted line in the high strain region (Figure 1A). Thus, the load−strain curve can be divided into three different zones: I, the zone prior to the strain-hardening zone; II, the strain-hardening zone; and III, the zone after the strain-hardening zone. Each zone has its unique feature in the structural development.

Zone I. Development of Mesophase (Precursor to Crystallization) before Strain-Hardening. In zone I, three WAXD images (nos. 1−3) were collected. The no. 1 pattern, taken before deformation, showed only an amorphous ring, confirming the randomly oriented initial structure. Upon deformation, a small increase in load was seen. This load remained at a constant level (8 N) in the remainder of zone I until the onset of the strain-hardening zone II (ca. 140% strain) was reached. The region of constant load is often referred to as the "*plastic deformation*" region. The no. 3 image exhibited a weak but distinct anisotropic pattern with no detectable crystalline reflections, representing the oriented mesomorphic pattern. The mesophase structure has a degree of packing order that is between the crystalline phase and the amorphous phase. On the basis of the no. 3 image alone, we cannot determine the exact type of mesophase (e.g., nematic or smectic) in the deformed sample. In the plastic deformation region, although the applied load stays about constant, the corresponding stress is increased rapidly due to the decrease of the cross-section area. This led to increases in both the degree as well as the fraction of oriented chains. The increasing molecular orientation in the plastic deformation of PET has been reported by several groups before using IR[9] and Raman[10] techniques and was also confirmed by Gorlier et al.[7] and Blundell et al.[2b] using X-ray methods. The fractions of the oriented mesophase as well as the oriented crystalline phase and random amorphous phase were estimated using a method[11] similar to the 2D analytical technique published earlier,[4] which is illustrated in Figure 2A. It is seen that in zone I, only oriented mesophase was developed, which increased with strain. The initial increase of the load in zone I represents the force needed to overcome the activation energy for polymer flow.[12] We speculate that the deformation-induced oriented mesophase has resulted from the orientation of chains with longer relaxation times (e.g., chains with higher molecular weight[13] and/or branched chains with strong local interactions) and the oriented molecules are segregated into distinct domains. In Figure 1B, the position of the amorphous peak in the

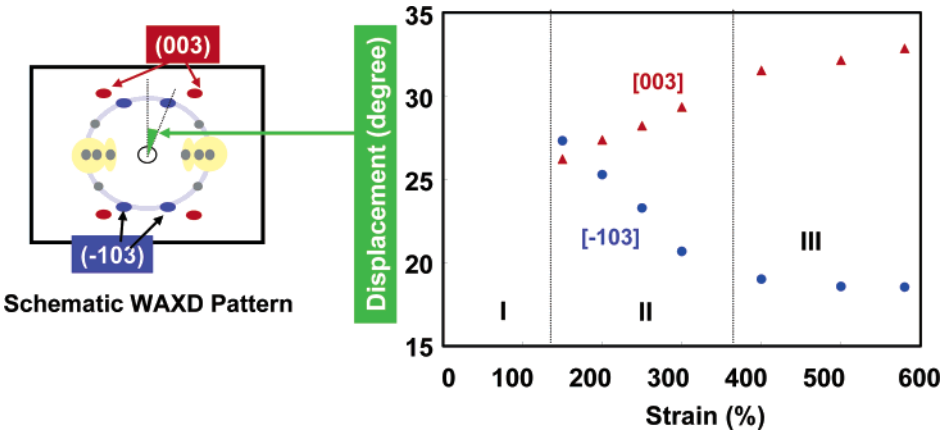

Figure 3. Schematic WAXD pattern illustrating the peaks of (003) and (−103) (left) and the displacement angles of diffraction peaks (003) and (−103) during deformation at 90 °C (right).

meridian was found to shift toward a smaller angle and the corresponding intensity was decreased, suggesting that the isotropic chains in the strained sample are more densely packed than the isotropic chains in the unstrained sample. We believe that the morphology of the deformed sample consists of an assembly of heterogeneous phases (mesomorphic and amorphous) instead of a homogeneous phase. Asano recently showed that the smectic phase formed a long-range layered structure using the SAXS technique.[3] We have also carried out extensive SAXS measurements during the formation of the mesophase, which will be a subject for discussion elsewhere.

At the end of zone I, the mesophase was found to decrease upon the initiation of crystallization, which supports the hypothesis that the mesophase acts as a *precursor* for crystallization even above T_g. Recently, we have reported that the smectic C structure behaved as a precursor for crystallization during deformation of PET below T_g based on the observation that the intensity of (001′) peak on the meridian decreased as the triclinic crystal structure developed.[2,3] In this study, we could not detect the existence of (001′), and thus the nematic structure might be dominant in the strain-induced mesophase above T_g. However, in the context of this work, we cannot exclude the existence of smectic C prior to crystallization. It is conceivable that the fraction of the smectic C structure was too small to be detected by WAXD since the total amount of the mesophase was relatively small to start with in this zone. The minimum concentration of the mesophase at which crystallization was induced under the chosen experimental conditions (90 °C, deformation rate = 20% strain/min) was about 20%. A similar mesophase behavior reported in the recent studies of high-speed spinning of PET[11] also supports this conclusion.

Zone II. Crystalline Perfection in the Strain-Hardening Zone. The strain-hardening zone is defined as the region between 140% and 380% strain; the corresponding images in Figure 1A are from no. 4 to no. 7. The no. 4 image showed a clear indication of crystallization, which coincided with the initiation of strain hardening. This was also reported in the studies of Gorlier et al.[7] and Salem.[6] A closer examination of the crystalline structure developed in this region revealed some new insights into the process of deformation-induced crystallization in PET.

Figure 3 shows that the displacements of two reflections (−103) and (003) change continuously with the applied strain. The displacement was defined as the azimuthal angle between the peak position and the meridional axis after correcting the effects of the curvature of the Ewald sphere using the Fraser's method.[14,4] It was found that the displacement of the (−103) peak decreased, while that of the (003) peak increased with strain. The changes in the azimuthal displacements of these reflections can be attributed to the deformation and/or the rotation of the PET unit cell. The effect of the unit cell rotation can be evaluated as follows. If the molecule axis (i.e., the crystallographic *c* axis) is tilted with respect to the fiber axis (which is actually known to occur in some samples of PET), while both crystallographic *a** and *b** axes remain perpendicular to the *c* axis, then as a consequence of the tilt, either the (*h*00) or the (0*k*0) and most likely the mixed (*hk*0) reflections on the equator should split up and show a bimodal azimuthal distribution. This feature was not seen in the WAXD patterns; thus, the effect of unit cell rotation must be very small. As a result, we have neglected the unit cell rotation as a possible source for the changes of the (−103) and (003) azimuthal displacements.

Concerning the unit cell deformation, the triclinic PET unit cell offers six adjustable lattice parameters. Our strategy to analyze the unit cell deformation was as follows. The majority of the parameters were kept constant at their ideal values in the stable crystalline PET structure. In addition, the changes of unit cell angles by shearing deformation were assumed to be more prompt to occur than the changes of unit cell dimensions by deforming crystalline chains. We found that a good description of the azimuthal changes in (−103) and (003) could be obtained by keeping *a*, *b*, *c*, and γ constant (a = 4.56 Å, b = 5.94 Å, c = 10.75 Å, and γ = 112 °)[15] and using α and β as variables. This approach gave us two variables to solve with two observable quantities. This approach is acceptable in this study because we are not too concerned with the precise determination of the deformed lattice constants, rather, we are looking for clues of the molecular mechanisms taking place during the process of strain-induced crystallization. In other words, while the actual values of *a*, *b*, *c*, and γ may vary slightly during stretching, the changes in α and β are the most dominant parameters in zone II. The changes of α and β are shown in Figure 4. It was seen that the β angle increased while the α angle decreased in zone II. The β shift represented the sliding of the (100) plane or the benzene ring in the

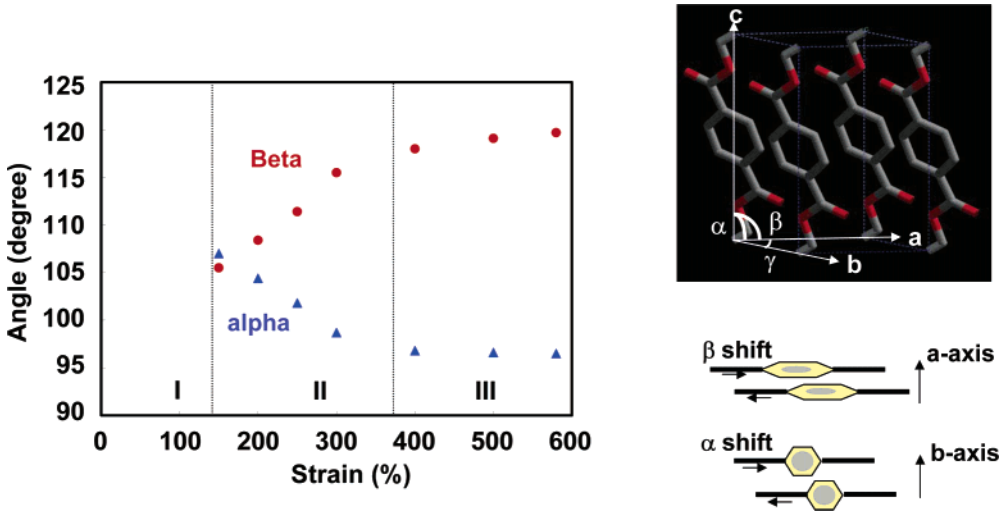

Figure 4. Changes of α and β angles in the unit cell during deformation (left) and the schematic diagram of PET triclinic unit cell structure calculated by Cerius 2 (lattice parameters: $a = 4.56$ Å, $b = 5.94$ Å, $c = 10.75$ Å α = 98.5°, $\beta = 118°$, $\gamma = 112°$[15]) as well as the molecular diagrams representing the α and β shifts.

unit cell. The initial value of β (105°) was between 90° and the equilibrium value (118°) in the triclinic structure, suggesting that the benzene molecules stacked more perpendicularly to each other at the initial stage of crystal formation. With the increase in strain, the benzene molecules slipped past each other probably due to the shearing motion and eventually settled into a stable triclinic structure as typically reported in the literature.[16]

Upon the initiation of crystallization, the applied load increased immediately. The load increase can be attributed to the formation of a three-dimensional (3D) network of imperfect crystallites, immersed in a continuous matrix containing random amorphous phase and oriented mesophase. The greater the concentration of the crystallites became, the larger the load developed. The crystal registration along the benzene sheet, which was indicative of the (010) peak, appeared to form first, whereas the growth along the benzene stacking direction appeared to develop later (see Figure 1B). During this zone, several processes seemed to proceed simultaneously with increasing strain: the crystal growth along all three directions, the crystal perfection and the crystal orientation. The crystal perfection process can be primarily followed by the changes of two unit cell angles (α and β) in the triclinic structure as discussed earlier. Finally, the end of zone II can be marked by the stabilization of the crystal structure and concentration, where the load is found to be linearly proportional to strain afterward.

Zone III. Stable Crystallization Development after the Strain-Hardening Zone. Zone III is defined as a region between 380% and 580% strain (the sample breaking point). In Figure 2A, both fractions of crystalline and mesophase increased and that of amorphous decreased with strain in this zone. It is thought that the mesophase was continuously developed from the isotropic amorphous phase and was converted into the stable crystalline structure by strain. In Figure 4, the changes in unit cell parameters α and β were found to be very small in zone III, suggesting that the crystal perfection process was largely completed in zone II. In other words, relatively few changes were seen in the crystalline structures developed in zone III, although notable increases in the fractions of crystalline phase and mesophase (Figure 2A) were observed. These results are somewhat different from the earlier studies by other research groups. For example, Gorlier et al. reported that the 3D crystalline growth started at the onset of the linear stress development, which coincided with the appearance of the (−103) peak indicating the ordering along the tensile axis.[7] Our result indicated that the 3D crystalline growth started at the beginning of zone II. After the perfection of the 3D crystalline structures, stable crystalline growth occurred in zone III. Salem reported that the crystallization process, estimated by the density measurement, slowed at the onset of the linear stress development.[6] In contrast, our study indicated that the mass fraction of the crystalline phase was found to increase almost linearly in zone III (Figure 2A). Perhaps the difference was due to their inclusion of the mesophase as part of the crystalline phase in the calculation.

The characteristics of zone III involve the linear relationship between the load and the strain until the break point is encountered. In this zone, the crystalline structure appears to be stable with increasing strain, having good crystallographic registrations typical of the PET triclinic unit cell. The increase in the load can be attributed to the simultaneous increases in both crystalline and mesomorphic fractions, which are probably initiated from the 3D crystalline network of stable structures developed at the end of zone II. Again, we speculate that the mesophase was induced by the orientation of the chains connected between the adjacent crystallites, while further crystallization took place in the mesophase. Although the overall crystal fraction was found to increase with strain, the presence of increasing mesophase fraction indicated that not all the oriented mesomorphic chain can be converted into the crystalline phase at the chosen temperature.

4. Conclusion. An in situ study of structural development in amorphous poly(ethylene terephthalate) under uniaxial deformation above T_g (90 °C) was carried out using synchrotron WAXD. The results showed several new insights into this subject. The load−strain curve can be divided into three zones (I, II, III) with each zone having a unique structure and property relationship. Zone I represents the development of mesophase (a precursor for crystallization), where a

constant load with strain can be seen. Zone II represents the strain-hardening region, which is marked by the development of a three-dimensional network of imperfect crystallites and mesomorphic chains. Zone III represents the further formation of mesophase and the growth of a stable crystal phase, which is characteristic of a constant load−strain ratio.

Acknowledgment. The authors thank the Toray Industry in Japan, the NSF Center for Advanced Engineering Fibers and Films at Clemson University (EEC-9731680), and the NSF (DMR0098104) for the financial support of this project. The authors also thank Mr. Uchida from Toray for the synthesis of experimental PET samples.

References and Notes

(1) (a) Welsh, G. E.; Blundell, D. J.; Windle, A. H. *Macromolecules* **1998**, *31*, 7562. (b) Welsh, G. E.; Blundell, D. J.; Windle, A. H. *J. Mater. Sci.* **2000**, *35*, 5225. (c) Blundell, D. J.; Mahendrasingam, A.; Martin, C.; Fuller, W. *J. Mater. Sci.* **2000**, *35*, 5057.

(2) (a) Mahendrasingam, A.; Blundell, D. J.; Martin, C.; Fuller, W.; MacKerron, D. H.; Harvie, J. L.; Oldman, R. J.; Riekel, C. *Polymer* **2000**, *41*, 7803. (b) Blundell, D. J.; Mahendrasingam, A.; Martin, C.; Fuller, W.; MacKerron, D. H.; Harvie, J. L.; Oldman, R. J.; Riekel, C. *Polymer* **2000**, *41*, 7793. (c) Mahendrasingam, A.; Martin, C.; Fuller, W.; Blundell, D. J.; Oldman, R. J.; MacKerron, D. H.; Harvie, J. L.; Riekel, C. *Polymer* **2000**, *41*, 1217. (d) Blundell, D. J.; MacKerron, D. H.; Fuller, W.; Mahendrasingam, A.; Martin, C.; Oldman, R. J.; Rule, R. J.; Riekel, C. *Polymer* **1996**, *37*, 3303.

(3) Asano, T.; Balta-Calleja, F. J.; Flores, A.; Tanigaki, M.; Mina, M. F.; Sawatari, C.; Itagaki, H.; Takahashi, H.; Hatta, I. *Polymer* **1999**, *40*, 6475.

(4) Ran, S.; Wang, Z.; Burger, C.; Chu, B.; Hsiao, B. S. *Macromolecules* **2002**, *35*, 10102.

(5) Strobl G. *Eur. Phys. J.* **2000**, *E3*, 165.

(6) (a) Salem, D. R. *Polymer* **1992**, *33*, 3182. (b) Salem, D. R. *Polymer* **1992**, *33*, 3189.

(7) Gorlier, E.; Haudin, J. M.; Billion, N. *Polymer* **2001**, *42*, 9541.

(8) Chu, B.; Hsiao, B. S. *Chem. Rev.* **2001**, *101*, 1727.

(9) (a) Middleton, A. C.; Ducketti, R. A.; Ward, I. M.; Mahendrasingam, A.; Martin, C. *J. Appl. Polym. Sci.* **2001**, *79*, 1825. (b) Shen, D.; Long, F.; Wen, Z.; Qian, R. *Makromol. Chem.* **1991**, *192*, 301. (c) Siesler, H. W. *Adv. Polym. Sci.* **1984**, *21*, 55. (d) Gupta, V. B.; Ramesh, L.; Siesler, H. W. *J. Polym. Sci., Polym. Phys. Ed.* **1985**, *23*, 405. (e) Siesler, H. W. *Pure Appl. Chem.* **1985**, *57*, 1603.

(10) (a) Rodriguez-Cabello, J. C.; Merino, J. C.; Fernandez, M. R.; Pastor, J. M. *J. Raman Spectrosc.* **1996**, *27*, 23., (b) Rodriguez-Cabello, J. C.; Merino, J. C.; Quintanilla, L.; Pastor, J. M. *J. Appl. Polym. Sci.* **1996**, *62*, 1953.

(11) (a) Shimizu, J.; Sen'i-Gakkaishi, **1985**, *38*, 243. (b) Shimizu, J.; Kikutani, T.; Takaku, A.; Okui, N.; Senni-Gakkaishi, **1981**, *37*, T-135. **Analysis Protocol.** A one-dimensional peak fitting was performed to deconvolute the crystalline and amorphous peaks from the linear intensity profiles extracted from the 2D WAXD patterns of Figure 1A with Grams software by Galactic Industries. Each peak was fitted by a mixed function of Gaussian and Lorenzian, whose formula is $f_{MIX} = (1 - M)$ (Gaussian) $+ M$ (Lorenzian), where M is the Lorenzian ratio. The amount of the oriented crystalline phase was assumed to be proportional to the total area of the fitted (100), (010). and (−110) peaks from the linear equatorial profile, whereas the amount of the amorphous phase was the area of the linear meridional profile. (The contributions from the off-equatorial reflections were excluded.) The typical peak fitting results were shown in Figure 2B. The subtraction of both crystalline and amorphous from the total area of the equatorial profile was estimated as the amount of the mesophase. The mass fraction of the individual phase was taken as the ratio of the area for each phase to the total area of the equatorial profile. As the effects of the orientation in mesophase and crystalline phase are ignored, the calculated amounts of crystalline phase and mesophase were overestimated.

(12) Glasstone, S.; Laider, K. J.; Eyring, M. *The Theory of Rate Processes*; McGraw-Hill: New York, 1941.

(13) (a) Doi, M.; Edwards, S. F. *The Theory of Polymer Dynamics*; Oxford University Press: Oxford, England, 1986. (b) de Gennes, P. G. *Scaling Concepts in Polymer Physics*; Cornell University Press: Ithaca, NY, 1979.

(14) Fraser, R. D. B.; Macrae, T. P.; Millar, A.; Rowlands, R. J. *J. Appl. Crystallogr.* **1976**, *9*, 81.

(15) Daubery, R. D.; Bunn, C. W.; Brown, C. J. *Proc. R. Soc. London A* **1954**, *226*, 531.

(16) (a) Bhatt, G. M.; Bell, J. P.; Knott, J. R. *J. Polym. Sci., Polym. Phys. Ed.* **1976**, *14*, 373. (b) Sauer, T. H.; Wendorff, J. H.; Zimmermann, H. J. *J. Polym. Sci., Polym. Phys. Ed.* **1987**, *25*, 2471. (c) Sun, T.; Zhang, A.; Li, F. M.; Porter, R. S. *Polymer* **1988**, *29*, 2115.

MA034791B